Whole field measurement of temperature in water using two-color laser induced fluorescence

J. Sakakibara, R. J. Adrian

Abstract A technique is described that measures the instantaneous three-dimensional temperature distribution in water using two-color laser-induced fluorescence (LIF). Two fluorescent dyes, Rhodamine B and Rhodamine 110, are used as temperature indicators. A laser light sheet scanned across the entire measurement volume excites the fluorescent dye, and an optical system involving a color beam splitter gives the intensity distribution of the individual fluorescent dyes on two separate monochrome CCD cameras. The ratio of these fluorescence intensities at each point of the image is calibrated against the temperature to eliminate the effect of the fluctuation of illuminating light intensity. A stable thermally stratified layer was measured by this system to evaluate the total accuracy of the measurement system. The random error of the measurement was ± 1.4 K with 95% confidence. Measurements of thermal convection over a heated horizontal surface show temperature iso-surfaces having typical structures such as plumes, ridges and thermals.

1
Introduction

While techniques such as particle image velocimetry are relatively well developed for the measurement of velocity fields, there are many flows in which the temperature field is of equal or even greater importance than the velocity. These flows range from thermal convection, in which buoyancy is the primary motive force, to forced convection in which heat transfer is the primary concern. In addition to being a fundamental thermophysical variable, temperature, being a scalar, is also a simple marker that is often very useful for visualizing the structure of the flow field, especially in three dimensions. This paper describes an improved method of measuring the temperature

J. Sakakibara[1], R. J. Adrian
Department of Theoretical and Applied Mechanics, University of Illinois at Urbana-Champaign, Urbana, IL 61801, USA

[1]*Present address*: University of Tsukuba, Tsukuba 305, Japan

Correspondence to: R. J. Adrian

field in water on planar domains and, by scanning, on volumetric domains, using laser induced fluorescence. Various techniques have been used previously to obtain the spatial distribution of the temperature in water. Thermo-chromic liquid crystals (TLC) are commonly used to visualize temperature qualitatively, and several researchers have reported quantitative measurements (Akino et al. 1988; Dabiri and Gharib 1991; Fujisawa et al. 1997). The color of white light scattered from the TLC particle can be calibrated against temperature and scattering angle. It is now possible to obtain quite sensitive TLC which change color from red to blue in a range of 1 K or less. However, the accuracy relative to the measurement range is not large. The uncertainty found in our experiments (95% confidence) is approximately 0.1 K with an available measurement range of 0.7 K.

Instead of using TLC, temperature-sensitive fluorescent dyes excited by laser light can also be used as a whole-field temperature diagnostic (Nakajima et al. 1990; Sakakibara et al. 1993, 1997; Satoh and Kasagi 1997). Here, the fluorescence intensity is proportional to the exciting light intensity and the concentration of the fluorescent dye. For some dyes, e.g. Rhodamine B, the fluorescence intensity depends on the temperature. This characteristic can be used to measure the temperature of the solvent if one can keep constant both the concentration and the exciting light intensity. The relative accuracy of this method is higher than that of the TLC method because it allows a wider range of variation of the temperature. Typically the accuracy is ± 1.5 K over a measurement range of 40 K or more. In practice, however, the exciting light intensity may vary due to several effects, including refraction of the light passing through the thermal field itself. This may cause significant error in the measurement. In order to overcome this problem, we propose a new technique which employs two fluorescent dyes whose emission intensities depend differently upon temperature. The ratio between the two fluorescence intensities is nearly independent of the incident light intensity. Our first report on this method was made in Sakakibara and Adrian (1997). The present work adds considerable depth to the knowledge needed to implement the techniques with good accuracy. We note that a similar temperature measurement strategy based on the use of Rhodamime B as the temperature dependent dye and disodium Fluorescin as a reference dye having a different temperature dependence has been reported recently by Oljaca and Glezer (1997).

We will explain the concepts and principles in Sect. 2, and the spectral characteristics of the fluorescent dyes, including temperature dependence and the quenching effect, will be discussed in Sect. 3. After showing the transmitting and

receiving optics and data acquisition system in Sect. 4, the accuracy of the method is characterized in Sect. 5, and an experimental result demonstrating the applicability of the method to natural convection over a heated horizontal surface will be shown in Sect. 6.

2 Principle

Fluorescence is a radiative decay process that occurs by electronic transitions in molecules. After a fluorescent dye molecule is exposed to an electromagnetic field, photons entering the molecule cause displacements of electrons from one region of the molecule to another. The displacement of electrons results in increased potential energy of the molecule from the ground state (S_0) to the first electronic excited state (S_1). When the energy state returns to the ground state, fluorescent light emission takes place as a radiative process. However, there are many non-radiative processes that can compete with the light emission and reduce the fluorescence efficiency. They depend on the structure of the molecule in a complicated fashion.

The ratio of the total energy emitted per quantum of energy absorbed by the molecule is called the quantum efficiency, ϕ. The fluorescence energy $I(\text{W m}^{-3})$ emitted per unit volume is defined as

$$I = I_0 C \phi \varepsilon \tag{1}$$

where I_0 is the incident light flux (W m^{-2}), C is the concentration of the dye solution ($\text{m}^{-3}\,\text{kg}$), and ε is an absorption coefficient ($\text{m}^2\,\text{kg}^{-1}$). In most organic dyes, the quantum efficiency ϕ is temperature dependent. The change in fluorescence intensity is normally small, usually less than a fraction of one per cent per K. However, the sensitivity of some compounds such as Rhodamine B can be as high as 2% K^{-1}. In contrast, the absorption coefficient, ε, does not have significant temperature dependence, being less than 0.05% K^{-1} here. Thus, it is possible to measure the temperature of the solution if one can keep the incident light flux, I_0, and concentration, C, constant.

As mentioned above, I_0 is affected by various agencies including convergence and divergence of the light sheet and (possibly time-dependent) refraction of the light passing through the thermal field. To avoid this problem, it is necessary to provide a means of measuring the local, instantaneous intensity of the illuminating light. This can be done using a fluorescent dye with a quantum efficiency that is not sensitive to temperature. This leads to the use of a mixture of two fluorescent dyes, called A and B whose quantum efficiencies differ. In addition, the two dyes should have different emission spectra so that the emitted light can be separated by optical means. If the two emission spectra can be perfectly separated by beam splitting optics (Fig. 1), then the individual intensities can be measured by two different cameras α and β, whose voltage outputs are V^α and V^β, respectively. The ratio

$$\frac{V^\alpha}{V^\beta} = \frac{I_A}{I_B} = \frac{C_A \phi_A \varepsilon_A}{C_B \phi_B \varepsilon_B} \tag{2}$$

is independent of the incident light flux I_0, but it can depend on temperature through the ratio ϕ_A/ϕ_B. In practice, imperfect
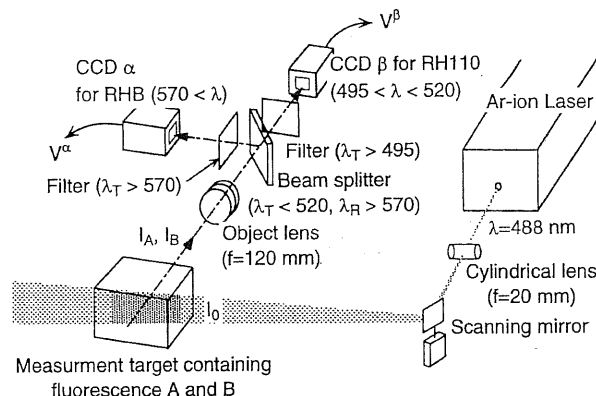

Fig. 1. Arrangement of the optical components

separation of I_A and I_B arises from the overlap of the emission spectrum of the two fluorescent dyes, and some fraction of I_A is detected by camera β, and some fraction of I_B is detected by camera α. In this situation, V^α and V^β can be expressed as

$$V^\alpha = F_A^\alpha I_A + F_B^\alpha I_B = I_0(F_A^\alpha C_A \phi_A \varepsilon_A + F_B^\alpha C_B \phi_B \varepsilon_B) \tag{3}$$

$$V^\beta = F_A^\beta I_A + F_B^\beta I_B = I_0(F_A^\beta C_A \phi_A \varepsilon_A + F_B^\beta C_B \phi_B \varepsilon_B) \tag{4}$$

where F_A^α and F_A^β are a fractions of the light I_A coming into the cameras α and β, respectively, and similarly for F_B^α and F_B^β. These fractions can be determined by making the concentration of one fluorescent dye zero and measuring the intensity of the light using the cameras. Let primes denote the property values extant during two experiments, one with $C_A = 0$ and the other with $C_B = 0$. For the case in which $C_B = 0$, $C_A = C_A'$, $I_0 = I_0'$, $\phi_A = \phi_A'$ and $\phi_B = \phi_B'$. Then F_A^α and F_A^β can be determined as

$$F_A^\alpha = \frac{V_{C_B=0}^\alpha}{I_0' C_A' \phi_A' \varepsilon_A}, \quad F_A^\beta = \frac{V_{C_B=0}^\beta}{I_0' C_A' \phi_A' \varepsilon_A} \tag{5}$$

Also, by making $C_A = 0$, $C_B = C_B'$, $I_0 = I_0'$, $\phi_A = \phi_A'$ and $\phi_B = \phi_B'$,

$$F_B^\alpha = \frac{V_{C_A=0}^\alpha}{I_0' C_B' \phi_B' \varepsilon_B}, \quad F_B^\beta = \frac{V_{C_A=0}^\beta}{I_0' C_B' \phi_B' \varepsilon_B} \tag{6}$$

Substituting Eqs. (5) and (6) in Eqs. (3) and (4), the ratio between V^α and V^β becomes

$$\frac{V^\alpha}{V^\beta} = \frac{C_A C_B' \phi_A \phi_B' V_{C_B=0}^\alpha + C_B C_A' \phi_B \phi_A' V_{C_A=0}^\alpha}{C_A C_B' \phi_A \phi_B' V_{C_B=0}^\beta + C_B C_A' \phi_B \phi_A' V_{C_A=0}^\beta} \tag{7}$$

Here, the four values $V_{C_A=0}^\alpha$, $V_{C_B=0}^\alpha$, $V_{C_A=0}^\beta$ and $V_{C_B=0}^\beta$ are constants once the optical system is fixed. The relationship between temperature and ϕ_A, ϕ_B is dye-dependent and measurable. Therefore, the intensity ratio V^α/V^β will be a function of C_A, C_B and temperature.

By denoting the concentration ratio as $C_{A/B} = C_A/C_B$, Eq. (7) can be expressed as

$$\frac{V^\alpha}{V^\beta} = \frac{C_{A/B} C_B' \phi_A \phi_B' V_{C_B=0}^\alpha + C_A' \phi_B \phi_A' V_{C_A=0}^\alpha}{C_{A/B} C_B' \phi_A \phi_B' V_{C_B=0}^\beta + C_A' \phi_B \phi_A' V_{C_A=0}^\beta} \tag{8}$$

8

The concentration ratio $C_{A/B}$ could also affect the temperature sensitivity of V^α/V^β which can be evaluated by differentiating Eq. (8) by T,

$$\frac{\partial}{\partial T}\left(\frac{V^\alpha}{V^\beta}\right)$$

$$=\frac{C_A'\phi_A'C_{A/B}C_B'\phi_B'(V_{C_B=0}^\alpha V_{C_A=0}^\beta - V_{C_A=0}^\alpha V_{C_B=0}^\beta)\left(\phi_B\frac{\partial\phi_A}{\partial T}-\phi_A\frac{\partial\phi_B}{\partial T}\right)}{(V_{C_B=0}^\beta C_{A/B}C_B'\phi_B'\phi_A + V_{C_A=0}^\beta C_A'\phi_A'\phi_B)^2}$$

$$(9)$$

If ϕ_A and ϕ_B are comparable, good sensitivity to temperature is obtained when the temperature dependency of ϕ_A and ϕ_B differs significantly;

$$\frac{d\phi_A}{dT}\gg\frac{d\phi_B}{dT}\quad\text{or}\quad\frac{d\phi_A}{dT}\ll\frac{d\phi_B}{dT}\qquad(10)$$

3
Fluorescence characteristics

3.1
Selection of the fluorescent dyes

Since $d\phi/dT$ is negative for most organic fluorescent dyes, a practical method of satisfying Eq. (10) is to choose one fluorescent dye with strong temperature dependence and the other fluorescent dye with little or no temperature dependence. Also, the emission spectra should differ enough to permit the separation of the emitted light by optical means.

Rhodamine B (RhB) has been selected as a temperature-sensitive dye for the present work, because its temperature sensitivity, (2.3% K^{-1}), is large and its absorption spectrum covers the range of 470–600 nm, making excitation easy by conventional visible lasers, e.g. Argon-ion, Nd-YAG, etc. RhB belongs to the group of Xanthene dyes which has three benzene rings; it is commonly used as a laser dye for wavelengths near 610 nm.

Candidates for the non-temperature-sensitive dye must have an absorption spectrum similar to RhB but a different emission band. Coumarine dyes, which have two benzene rings instead of three, have satisfactory spectra ($\lambda_{abs}=455$ nm, $\lambda_{em}=497$ nm for Coumarine 6), and they are less sensitive to temperature than RhB. However, Coumarine dyes are not soluble in water. Of the Xanthene dyes which are water soluble. Fluorescein has short wavelength absorption and emission ($\lambda_{abs}=498$ nm, $\lambda_{em}=518$ nm in methanol). However, Fluorescein in fairly temperature dependent (0.6% K^{-1}). Another Xanthene dye Rhodamine 110 (Rh110), has similar spectral characteristics ($\lambda_{abs}=496$ nm, $\lambda_{em}=520$ nm), and its temperature dependence is much smaller (0.13% K^{-1}). Hence we have chosen Rh110 as the non-temperature-sensitive dye.

The basic characteristics of RhB and Rh110 in water at $T=20$ °C are summarized in Table 1. RhB (Aldrich, dye content >80%) and Rh110 (Acros, laser grade) were used without further purification. Following the method described in (Guilbault 1973) to determine the quantum efficiency, the value of ϕ for Rh110 was found by measuring the fluorescence intensity of Rh110 relative to that of RhB, as reported in Arbeloa et al. (1991).

3.2
Spectral characteristics

Figure 2 shows the absorption spectra of RhB (1.0 mg l^{-1}) and Rh110 (1.0 mg l^{-1}), and the emission spectrum of the mixture of these dyes (RhB: 2.0 mg l^{-1}, Rh110: 0.2 mg l^{-1}) measured by a spectrometer (Jobin Yvon, 270M) with a CCD camera (Sony, XC77) as a detector. The exciting light wave-length for the emission spectra measurement was $\lambda_{ex}=488$ nm, and the solvent was deionized water for both absorption and emission measurements.

Emission occurs at a longer wavelength than absorption because the emissive transition occurs after some vibrational energy has been lost into surrounding molecules of the solvent (Atkins 1994). The shape of the emission spectrum of the mixture of the dyes is similar to that of the simple summation of individual dye's spectra (not shown here). As expected, the emission spectrum at $T=25$ °C has a larger value than that of $T=29$ °C at the wavelength of maximum RhB emission ($\lambda=575$ nm), and less difference at the maxima of Rh110 emission spectra ($\lambda=520$ nm). Note that a shift of the emission spectrum due to the change of the temperature, such as that
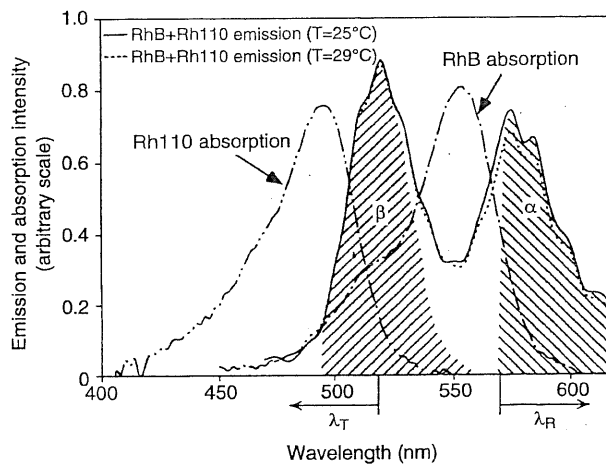

Fig. 2. Emission and absorption spectra of a mixture of RhB and Rh110 ($C_{RhB}=2.0$ mg l^{-1}, $C_{Rh110}=0.2$ mg l^{-1})

Table 1. Basic characteristics of RhB and Rh110 (Solvent: de- ionized water, T=20 °C)

Dye	Molecular weight	λ_{abs} [nm]	λ_{em} [nm]	ϕ	$\varepsilon_{\lambda=488}$ [m^2 g^{-1}]	$\varepsilon_{\lambda=\lambda_{abs}}$ [m^2 g^{-1}]	$\varepsilon_{\lambda=\lambda_{Rh110}}$ [m^2 g^{-1}]
RhB	479.02[Jones 1990]	554	575	0.31[Arbeloa et al. (1991)]	4.4	1.1	5.8
Rh110	366.80[Jones 1990]	496	520	0.8	34	0.073	1.1

which occurs in quinine sulfate (Guilbault 1973), was not observed.

The maxima of the absorption and emission spectra are almost evenly spaced approximately 30 nm apart. Since the overlapping region of each absorption spectrum ranges from 480 to 530 nm, the exciting light wavelength λ_{ex} should be in this range to excite both dyes at the same time. It seems appropriate to choose a wavelength at the middle of this range, e.g. $\lambda_{ex} = 514.5$ nm of Argon-ion laser, as the exciting light wavelength. However this wavelength almost matches the wavelength of maxima Rh110 emission, and we need to be able to separate the exciting light and emitted light by a long wave pass filter in the receiving optics, in order to eliminate the scattered light from the measurement volume. Thus, we chose the $\lambda_{ex} = 488$ nm line of Argon-ion laser as the exciting light wavelength in this study, instead of the 514.5 nm line.

3.3
Temperature dependence

Figure 3 shows the temperature variation of the fluorescence intensity of RhB (5.0×10^{-2} mg l^{-1}), I_{RhB}, and Rh110 (2.5×10^{-3} mg l^{-1}), I_{Rh110}, after being transmitted through our system of filters and splitter. The intensity is normalized by its value at $T = 20$ °C. In the measurement, dye solution was contained in a glass cuvette (Spectrocell, 3.5 ml, 10 mm path) held by a copper cuvette holder soldered onto a copper pipe. Temperature of the dye was varied by changing the temperature of the water flowing through the copper pipe. In order to make the temperature of the dye solution in the cuvette uniform, the fluid in the cuvette was stirred by a tiny rotating glass plate. Temperature was measured by a glass-coated thermistor probe and a digital multi-meter. Fluorescence intensity was measured by the CCD camera. The temperature was increased and then decreased over a range from 15 °C to 40 °C.

The intensity change of RhB is repeatable and significant, especially at lower temperatures. In contrast to RhB, the fluorescence intensity of Rh110 is very nearly constant. The temperature dependencies of RhB and Rh110 are, respectively, 2.3% and 0.13% K^{-1} at 20 °C.
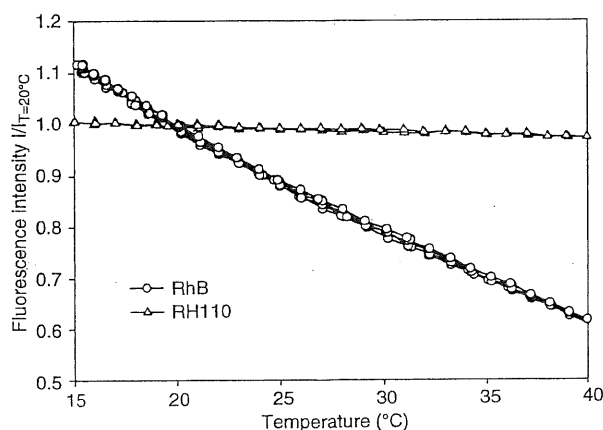
According to Drexhage (1977) the strong temperature dependence of RhB is attributed to the mobility of the amino groups in the dye molecule. The amino groups are rotated by the thermal energy of the solvent molecules, and rotation is enhanced with increasing temperature. In fact, one fluorescent dye, Pyronin B, which has diethyl amino groups, but no carboxylphenyl substituent, also has strong temperature dependency. If these groups do not exist, as in Rh110, or are rigidized, as in Rhodamine 101, the fluorescence quantum yield is almost independent of temperature.

The relationships between temperature and the quantum efficiency ϕ_{RhB} and ϕ_{Rh110} were obtained from values at $T = 20$ °C (see Table 1) as follows.

$$\phi_{RhB}(T) = \phi_{RhB}(T=20\,°C)\frac{I_{RhB}(T)}{I_{RhB}(T=20\,°C)} \qquad (11)$$

$$\phi_{Rh110}(T) = \phi_{Rh110}(T=20\,°C)\frac{I_{Rh110}(T)}{I_{Rh110}(T=20\,°C)} \qquad (12)$$

Note that the temperature dependence of the absorption coefficient is less than 0.05% K^{-1} for either fluorescent dye.

3.4
Quenching

In Sect. 3.3 the temperature dependences of the fluorescence intensity of RhB and Rh110 were discussed. Fluorescence, however, may be degraded by several other effects.

The most noticeable effect is the degradation of the fluorescence intensity caused by too much exciting light. Figure 4 shows the fluorescence intensity of RhB (5.0×10^{-2} mg l^{-1}) and Rh110 (2.5×10^{-3} mg l^{-1}) in response to an on-off sequence of the exciting light. The dyes were contained in a planar glass cuvette ($2 \times 25 \times 45$ mm^3) to prevent significant circulation of the fluid, and a laser light sheet ($1/e$ thickness and width were 10.2 and 0.89 mm, respectively) illuminated the fluid in the cuvette. The laser light was turned on for 50 s, then turned off 50 s, and this cycle was repeated while the power of the laser was increased. The fluorescence intensity at the middle of the sheet, the brightest
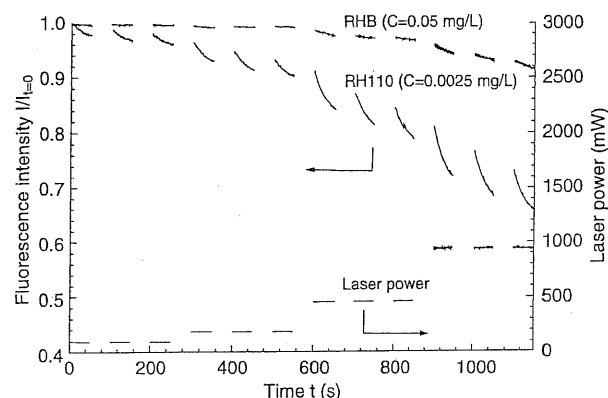
Fig. 3. Variation of the fluorescence intensity against temperature

Fig. 4. Time evolution of the fluorescence intensity of RhB (5×10^{-2} mg l^{-1}) and Rh110 (2.5×10^{-3} mg l^{-1}) with intermittent excitation
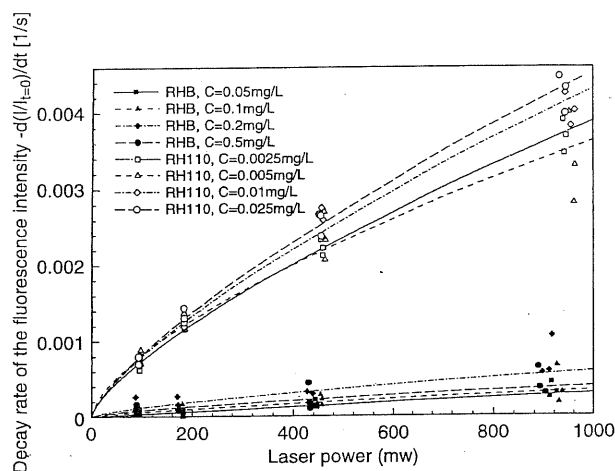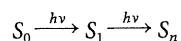
Fig. 5. Decay rate of the fluorescence intensity at the beginning of the excitation

Fig. 6. Time evolution of the fluorescence intensity of RhB with glass or fluoropolymer-encapsulated stirring bar

region, was detected by a photo-diode (BS 500B, Sharp) with a filter which transmitted the wavelengths larger than 495 nm. In Fig. 4 the fluorescence of Rh110 decreased rapidly after the excitation started, and decayed exponentially. The effect is stronger at larger exciting light intensity. RhB also has the same tendency, but the degradation is less than that of Rh110. It is interesting that the fluorescence intensity partially recovers after turning off the light.

The decay rate at the beginning of excitation is plotted in Fig. 5. With increasing laser power the decay rate increases monotonically. The degradation is caused by an increase of the population of non-fluorescent molecules which are produced by photo-chemical reactions (Jones 1990). It can be explained by a two-photon excitation process. High light flux causes an extra photon input after the transition to the upper state (S_1), and then further transition occurs to the next state (S_n).

$$S_0 \xrightarrow{h\nu} S_1 \xrightarrow{h\nu} S_n$$

Molecules in state S_n must be considered as potentially reactive intermediates which can be deleterious.

The other effect is degradation caused by impurity of the solution. Figure 6 shows the time evolution of the fluorescence intensity of RhB in a glass cuvette (3.5 ml, 10 mm path, Spectrocell) stirred by either a glass or a fluoropolymer-encapsulated stirring bar. The time axis starts from the time when we put the fluorescence solution and stirring bar into the glass cuvette. When the fluoropolymer stirring bar was in the solution, the fluorescence intensity dropped rapidly just after the preparation, and then recovered asymptotically. This phenomenon was not observed for the glass stirring bar. Although we tried to clean the fluoropolymer stirring bar using a detergent prior to the measurement, the results were not as good as for the glass stirring bar. Possibly, some contaminants on the fluoropolymer stirring bar dissolved in the solution and chemical reactions took place. Consequently, we suggest using glass equipment for the actual measurement. Alternatively, the dye solution should be allowed to age for several hours after the initial preparation.
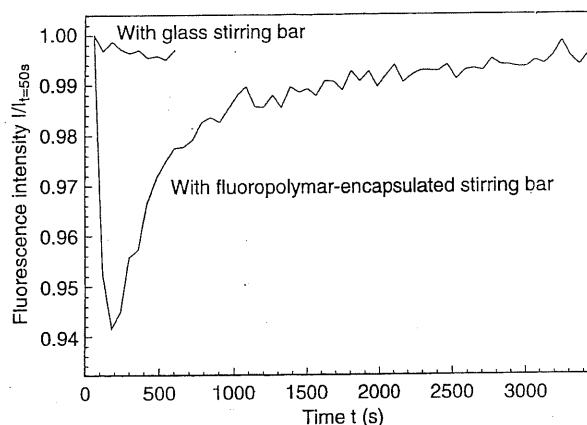
4
Measurement system and procedure

4.1
System configuration

The optical system consists of transmitting and receiving parts shown schematically in Fig. 1. In the transmitting part, a laser beam with a wavelength of $\lambda_{ex} = 488$ nm emitted from an Argon-ion laser (maximum power of 488 nm single line = 1.4 W, Coherent, Innova70) was expanded by a cylindrical lens ($f = -20$ mm) to form a laser light sheet in the flow field. The $1/e$ thickness and width of the sheet were 0.89 nm and 37 mm, respectively. A scanning mirror (General Scanning, 6325D) was used to sweep the light sheet in the out-of-plane direction. The scanner controller (General Scanning, CX660) was connected to a digital-to-analog convertor (National Instruments, LAB-PC) controlled by an IBM-PC compatible computer.

In the receiving optics, the fluorescent light was collected by a lens ($f = 120$ mm, F5.6, Nikon, Nikkor-AM*ED) and split by a dichroic beam splitter (CVI, SWP-45-R570- T520-PW2025C). The distance between the lens and the object plane was approximately 650 mm, and the magnification factor was 0.23. The physical size of the area of interest was 40×30 mm^2. At 45° incident angle the beam splitter transmitted wavelengths $\lambda_T \leqslant 520$ nm and reflected the wavelengths $\lambda_R \geqslant 570$ nm. Between these limits the transmittance and reflectance varied continuously. The transmitted light was passed through a filter that rejected wavelengths lower than 495 nm (Melles Griot, 03FCG067) to eliminate the Mie scattered light from particles in the flow. It was imaged onto CCD camera β (Sony, XC77). The reflected light was also passed through a filter that rejected wavelengths shorter than 570 nm (Melles Griot, 03FCG089) to eliminate the shorter wavelengths completely. It was imaged onto CCD camera α (Sony, XC77). The positions of the emission spectrum detected by cameras and are indicated by the cross-hatched regions in Fig. 7. It is clear that the CCD cameras α and β mainly detected the images of RhB and Rh110 emission, respectively.

The positions of each CCD camera were adjusted to capture the images of approximately the same area in the flow field.
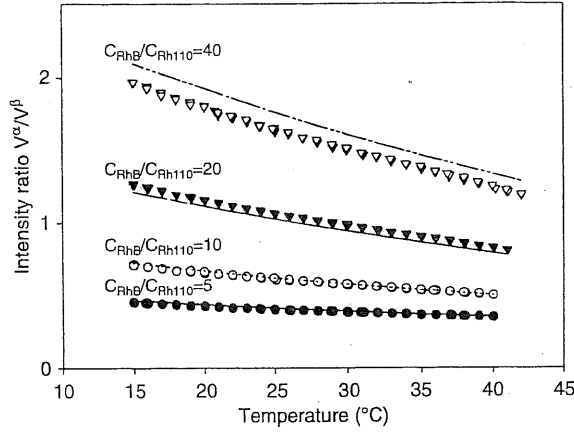
Fig. 7. Variation of the ratio between two CCD camera's output against temperature

Since we calibrated the physical coordinates and the image coordinates (see Sect. 4.2), further positioning of the cameras was not needed. The timings of the video signals of the CCD cameras were synchronized by sending the video signal of one CCD camera to the input for the vertical synchronization of the other CCD camera. The video signals from the CCD cameras were digitized by a frame grabber (Imaging Technology, IC-PCI) with three independent A/D channels, and transferred to the host memory of the PC at 30 frames per a second. The system was able to capture up to 44 successive frames (88 interlaced fields) in 1.46 s.

4.2
Calibration of image coordinates

To determine the correspondence between physical coordinates and image coordinates, we took images of a calibration plate which had a grid pattern with 1 mm intervals printed on a light-diffusive glass plate. The surface of the plate was set in the plane of the laser light sheet and illuminated from the back by a halogen lamp. The grid image was captured by each CCD camera through the receiving optics. The location of each grid point in the image plane coordinates was automatically obtained by finding local peaks of a cross-correlation function between the grid image and a template image which had a pattern of one grid. After obtaining the correspondence between the location of each grid point in the physical coordinate and that in the image coordinate, a 3rd-order polynomial function was fitted by the least-squares method. The image coordinate (X, Y) of the physical coordinate (x, y) was expressed as a function:

$$X = \sum_{i=0}^{3} \sum_{j=0}^{3} \xi_{ij} x^i y^j \qquad (13)$$

$$Y = \sum_{i=0}^{3} \sum_{j=0}^{3} \eta_{ij} x^i y^j \qquad (14)$$

Here, the coefficients ξ and η were obtained by the least-square method. This procedure compensated automatically for camera mis-alignment and distortion due to refraction by the optical interfaces. A similar procedure is discussed in detail in Soloff et al. (1997).

4.3
Variation of the intensity ratio against temperature

The variation of the intensity ratio V^α / V^β against temperature is shown in Fig. 7 as a function of the concentration ratio. The fluorescent dye was kept in the same cuvette mentioned in Sect. 3.3, and intensity was measured using the receiving optics described in the previous sections. In the figure, symbols represent the value measured experimentally, and the curves are the values evaluated from Eq. (7). Although the theoretical curves are in reasonable agreement with the experimental values, a slight disagreement, which might have originated from error in the concentration of the dyes, could cause a significant error in the measurement if we use this theoretical curve as the intensity ratio/temperature calibration curve directly. Therefore, we normalized the calibration curve to match the theoretical and experimental values at a 'reference' temperature, T_{ref}. For this procedure it is required to measure the intensity ratio at T_{ref} by making a uniform tempearture distribution in the flow field prior to the actual experiment.

Note that the calibration curve also depends on the location in the image, because the incident angle of the light path into the beam splitter affects the spectral characteristics of the transmitted and reflected incoming light. Therefore the intensity ratio vs. temperature calibration curves, including the four optical constants $V^\alpha_{C_A = 0}$, $V^\alpha_{C_B = 0}$, $V^\beta_{C_A = 0}$ and $V^\beta_{C_B = 0}$ in Eq. (7), should be obtained for each measurement point in the field of view.

In the Fig. 7 it is obvious that the concentration ratio, C_A / C_B, affects the intensity ratio and its sensitivity to the temperature (Eq. (9)). The value of V^α / V^β at 20 °C evaluated from the Eq. (8) is shown in Fig. 8 as a solid line with symbols representing the value obtained experimentally. The value of V^α / V^β increases monotonically with increasing C_{RhB} / C_{Rh110}. An optimum value of V^α / V^β exists according to the following reasoning. If the S/N ratio of either V^α or V^β was lower than the other, measurements of V^α / V^β could not have higher S/N ratio than that of the lower one. In other words, the S/N ratio of the measurements of V^α / V^β should be maximized when the S/N ratios of both V^α and V^β are equal. Since the sensitivities of the CCD cameras were set equal, the S/N ratio of each camera was the same when the V^α / V^β was unity. This condition was realized when $C_{RhB} / C_{Rh110} \simeq 20$, as shown in the Fig. 8.

Figure 9 shows the variation of the temperature sensitivity against the C_{RhB} / C_{Rh110}. It is observed that the maximum sensitivity (approximately 1.6–1.7% K^{-1}) can be realized in a range of C_{RhB} / C_{Rh110} from 20 to 40 in which the value of V^α / V^β is unity, as mentioned above. Thus, we used the concentration ratio of $C_{RhB} / C_{Rh110} = 20$ in our experiments.

5
Error estimates

To examine the random errors and bias errors, direct comparisons between the measured results and a thermistor probe were made with and without perturbation of the excitation light intensity distribution. The test field was a stable, thermally stratified layer. The test apparatus was a glass container (150 × 150 × 150 mm³) with an aluminum bottom (Fig. 10). The bottom surface was uniformly cooled by cold water and the top surface was uniformly heated by an electrical heater. The
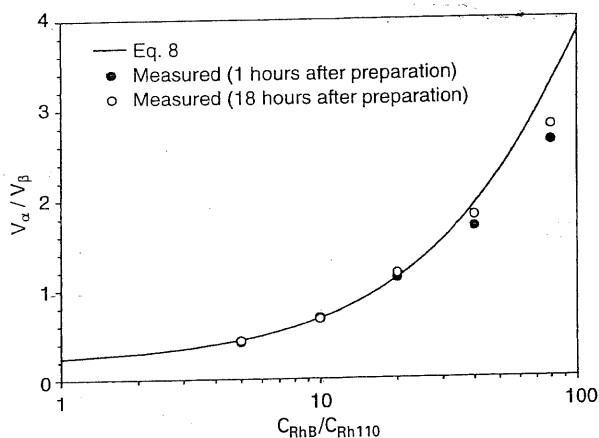
Fig. 8. Variation of the ratio between two CCD camera's output against the concentration ratio C_{Rh110}/C_{RhB}
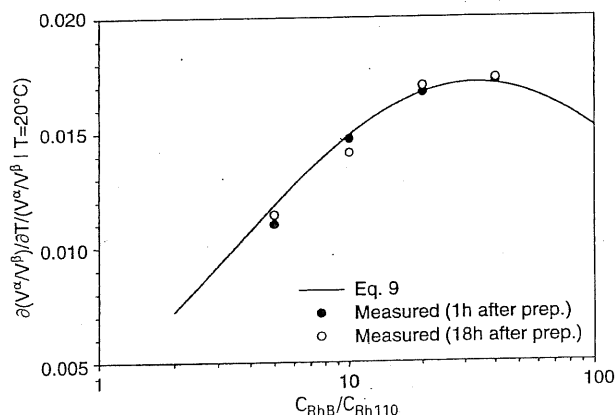

Fig. 9. Variation of the temperature sensitivity of ratio of the CCD cameras outputs against the concentration ratio C_{Rh110}/C_{RhB}
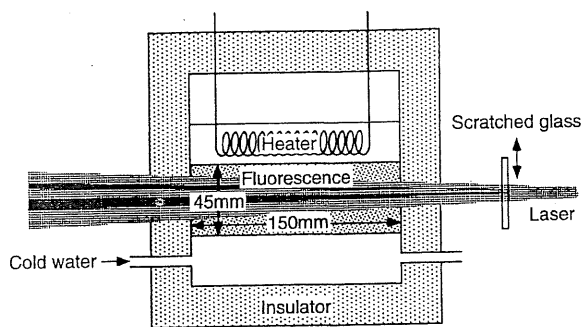

Fig. 10. Experimental apparatus for the stable thermally stratified layer

container was insulated by 50 mm of styrofoam. The fluorescent dye mixture was excited by a stationary laser light sheet. The dye concentrations were $C_{RhB} = 0.05$ mg l^{-1} and $C_{Rh110} = 0.0025$ mg l^{-1}.

The steady state vertical temperature profile was measured by a thermister probe and by LIF. To simulate fluctuations of the intensity distribution in the laser light sheet (which would be caused by changes of the refractive index in convective
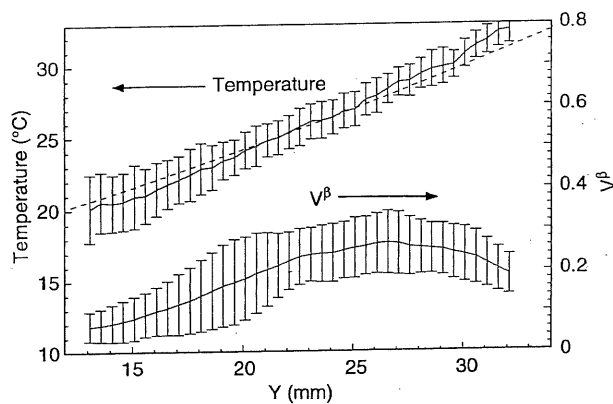

Fig. 11. Temperature profile of the stable thermally stratified layer. Laser light intensity is proportional to V^β
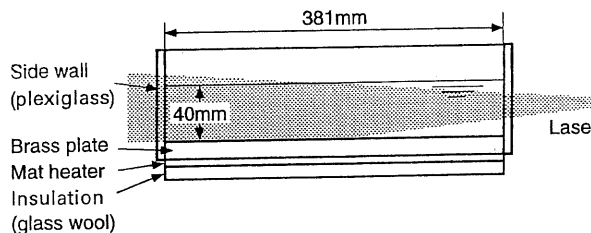
Fig. 12. Experimental apparatus for natural convection over a heated horizontal surface

conditions) the laser light intensity was perturbed by moving a scratched glass plate in the path of the illuminating laser beam.

In Fig. 11 a solid line and a dashed line show the ensemble-averaged temperature profiles measured by the LIF intensity ratio and the thermistor probe respectively. The number of data at each point was 294 and the error bars represent the range of four standard deviations (95% confidence) of the data.

The reference temperature, T_{ref}, was 23.0 °C. Both profiles agree within approximately ± 1 K. The LIF measurement appears to be biased systematically with respect to the thermistor probe. Over the height of the cell the illuminating beam intensity, as indicated by V^β, varied from 0.06 to 0.27, a factor 4.6:1. The random error was ± 1.0 K at the location where V^β was maximum, and it increased when the exciting light intensity decreased. The random error averaged over the whole measurement range was ± 1.4 K (95% confidence), and the maximum systematic error was 1.3 K. The random error was mainly caused by random noise in the CCD camera and the frame grabber.

6
Measurement of thermal convection from a heated horizontal surface

The two-color LIF technique was used to measure the three-dimensional temperature field of thermal convection from a horizontal surface with uniform heating. The test section consisted of a rectangular box heated from below by electrical mats bonded to the lower side of a smooth 12.7 mm thick brass plate, as shown in Fig. 12. The box was filled with de-ionized
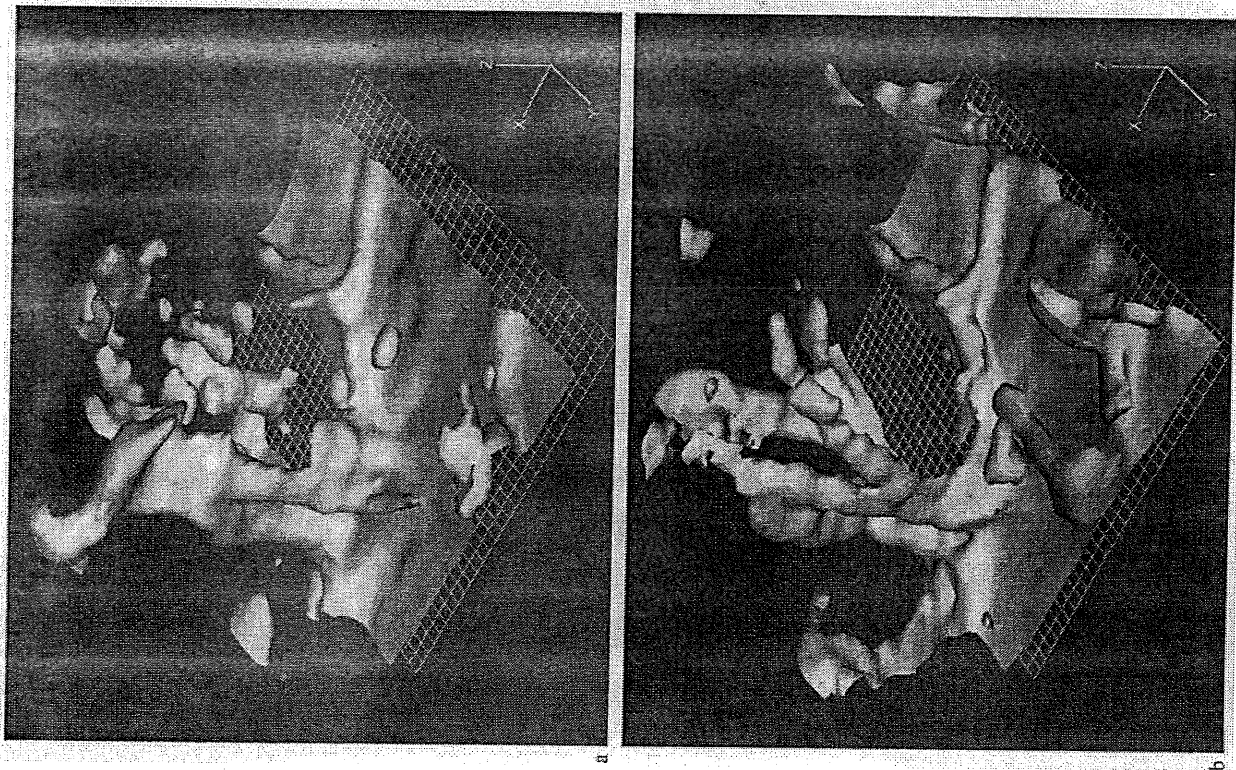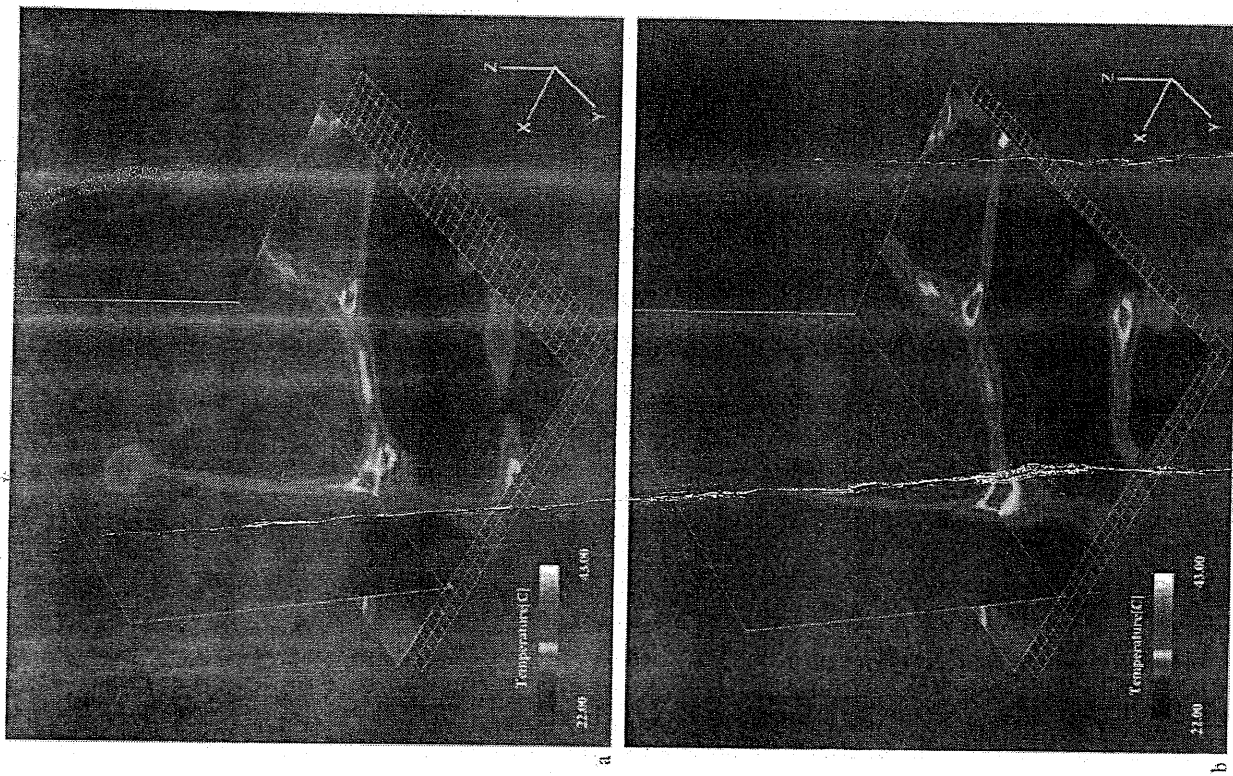
14

Fig. 14.

Fig. 13.

water with dye concentration of $C_{RhB} = 0.05$ mg l^{-1} and $C_{Rh110} = 0.0025$ mg l^{-1}. Its interior horizontal dimensions were 152 mm $\times$ 381 mm and $H = 40$ mm depth. The top of the fluid layer was a free surface. The mean heat flux supplied by the heater was 27 k W m^{-2} and the mean temperature drop from the heated surface to the center of the mixed layer was $\Delta T = 15$ K. The Raleigh number was $Ra = \beta g H^3 \Delta T / \alpha v = 1.3 \times 10^7$, where β is the thermal coefficient of expansion, g is gravity, and α is the thermal diffusivity. To obtain a quasi-three dimensional reconstruction of the temperature field, the laser light sheet was scanned 30 mm horizontally in a period of 0.73 s. Images were captured every 1/60th second, so the spatial interval of successive images was 0.7 mm. Figures 13a and 13b respectively show surfaces of constant temperature at time $t = 0.0$ and 0.73 s. Here the white grids represent the horizontal surface and the intervals are 1 mm each. The laser light sheet was parallel to the y-axis and swept in the direction of the x-axis. The flow field was dominated by turbulent structures having the forms of plumes and ridges. The plumes, which consist of columns of buoyant fluid rising up from the thermal boundary layer, connected to the ridges lying on the surface. These ridges originate from instabilities of the thermal boundary layer at the intersection of the cell, or nodes of the ridges.

Figure 14 shows the temperature distribution on a horizontal $(x - y)$ plane in the vicinity of the surface. This figure demonstrates the ability of the present technique to reconstruct $x - y$ data from successive $x - z$ data, albeit subject to small errors associated with evolution of the field during the scan time and refraction by turbulent temperature gradients. The temperatures at the nodes are much higher than in other parts of the ridges, or inside the cells. As the fluid inside a cell convects toward the ridges, the accumulation of the heat at the node makes the boundary layer thicker and creates more buoyancy at the node where the plumes rise upwards.

7
Conclusion
A new technique for the whole-field, non-intrusive measurement of water temperature has been described and demonstrated. It uses two fluorescent dyes, one to sense temperature and the other to sense the intensity of illumination. Rhodamine B was used for the temperature-sensitive indicator, and Rhodamine 110 was used for the non-temperature-sensitive indicator. The principal measured quantity is the ratio of the intensity of the light emitted by the Rhodamine B divided by the intensity of the light emitted by Rhodamine 110. This ratio is independent of variation of the illuminating beam intensity. Measurements of a stably stratified layer show that the random error was ± 1.4 K (95% confidence) and the maximum bias error was 1.3 K. The technique is simple enough to permit

reconstruction of three-dimensional temperature fields by scanning the light sheet. Application of the current technique to thermal convection over a heated horizontal surface shows typical structures in the form of plumes and ridges.

The present technique can be improved if a fluorescent dye having greater sensitivity can be found. The accuracy can also be enhanced by using cameras having 10- or 12-bit resolution with correspondingly less noise. The ideal pair of fluorescent dyes for these technique would have similar absorption spectra and non-overlapping emission spectra.

References
Akino N; Kunugi T; Ueda M; Kurosawa A (1988) Liquid-crystal thermometry based on automatic color evaluation and applications to measure turbulent heat transfer. Transport Phenomena in Turbulent Flows Theory, Experiment, and Numerical Simulation, (Hirata M; Kasagi N ed) 807–820. Hemisphere

Arbeloa TL; Estevez MJT; Arbeloa FL; Aguirresacona IU; Arbeloa IL (1991) Luminescence properties of rhodamines in water/ethanol mixtures. J Lumin 48 & 49: 400–404

Atkins PW (1994) Physical Chemistry. Freeman, New York

Dabiri D; Gharib M (1991) Digital particle image thermometry: the method and implementation. Exp Fluids 11: 77–86

Drexhage KH (1977) Structure and properties of laser dyes. In: Dye Lasers (ed. Schäfer, F.P.) Springer, Berlin, pp 144–193

Fujisawa N; Adrian RJ; Keane RD (1997) Three-dimensional temperature measurement in turbulent thermal convection over smooth and rough surfaces by scanning liquid crystal thermometry. Proc. Int. Conf. on Fluid Engineering, JSME Centennial Grand Congress, Tokyo, pp 1037–1042

Guilbault GG (1973) Practical fluorescence: Theory, methods, and techniques. Marcel Dekker, New York

Jones GH (1990) Photochemistry of Laser Dyes, in Dye Laser Principles with Applications (Durate FJ; Hillman LW eds) Academic Press, New York, pp 287–343

Nakajima T; Utsunomiya M; Ikeda Y; Matsumoto R (1990) Simulataneous measurement of velocity and temperature of water using LDV and fluorescence technique. 5th Int. Symp. on Appl. of Laser Tech. to Fluid Mech. Lisbon, 2.6.1–2.6.6

Oljaca M; Glezer A (1997) Measurement of aero-optical effects in a plane shear layer. AIAA Paper 97-2352, 28th Plasma Dynamics and Lasers Conf

Sakakibara J; Adrian RJ (1997) Measurement of whole-field temperature using two-color LIF. J. Visualization Soc. Japan 17: 333–336 (in Japanese)

Sakakibara J; Hishida K; Maeda M (1993) Measurements of thermally stratified pipe flow using image-processing techniques. Exp Fluids 16: 82–96

Sakakibara J; Hishida K; Maeda M (1997) Vortex structure and heat transfer in the stagnation region of an impinging plane jet (simultaneous measurement of velocity and temperature fields by DPIV and LIF). Int J Heat Mass Transfer 40, 13, 3163–3176

Satoh K; Kasagi N (1997) Combined velocity and scalar field measurement with the simultaneous use of scanning PIV and LIF. The 10th Int Symposium on Transport Phenomena in Thermal Science and Process Engineering (ISTP10) to be published

Soloff S; Adrian RJ; Liu Z (1997) Distortion compensation for generalized stereoscopic particle image velocimetry. Meas Sci Tech 8: 1441–1454

Fig. 13. Surfaces of constant temperature of natural convection over a horizontal heated surface. a $t = 0$ s and b $t = 0.73$ s (Fig on page 8 left)
Fig. 14. Iso-therms in a horizontal plane in the vicinity of the heated lower surface. a $t = 0$ s and b $t = 0.73$ s (Fig on page 8 right)